SATELLITE IMAGE FUSION

PROJECT REPORT

Submitted by

AISHWARYAA V D **Reg. No.:13BEC006**

ARAVIND KRISHNA C **Reg. No.:13BEC018**

in partial fulfilment for the award of the degree

of

BACHELOR OF ENGINEERING

IN

ELECTRONICS AND COMMUNICATION

KUMARAGURU COLLEGE OF TECHNOLOGY

COIMBATORE - 641 049

(An Autonomous Institution Affiliated to Anna University, Chennai)

ANNA UNIVERSITY : CHENNAI

APRIL 2017

BONAFIDE CERTIFICATE

Certified that this project report **"SATELLITE IMAGE FUSION" is the bonafide work of AISHWARYAA.V.D [Reg. No: 13BEC006] and ARAVIND KRISHNA.C [Reg. No: 13BEC018]**, who carried out the project work under my supervision. Certified further that to the best of my knowledge the work reported herein does not form part of any other project or dissertation on the basis of which a degree or award was conferred on an earlier occasion on this or any other candidate.

SIGNATURE
Dr. A. Vasuki , Ph.D.,
PROJECT SUPERVISOR
Department of ECE
Kumaraguru College of Technology
Coimbatore-641049

SIGNATURE
Dr. K. Malarvizhi , Ph.D.,
HEAD OF THE DEPARTMENT
Department of ECE
Kumaraguru College of Technology
Coimbatore- 641049

The candidates with Register No: 13BEC006 and 13BEC018 are examined by us in the project viva-voce examination held on ……

INTERNAL EXAMINAR **EXTERNAL EXAMINAR**

ACKNOWLEDGEMENT

We express our sincere thanks to the Management of Kumaraguru College of Technology and Joint Correspondent **Shri. Shankar Vanavarayar** for the kind support and for providing necessary facilities to carry out the project work.

We would like to express our sincere thanks to our beloved Principal **Dr. R.S.Kumar,** Kumaraguru College of Technology, who encouraged us in each and every step of the project.

We would like to thank **Dr. K. Malarvizhi,** Head of the Department, Electronics and Communication Engineering, for her kind support and for providing necessary facilities to carry out the project work.

We wish to thank with everlasting gratitude to our Project Coordinator **Prof. S. Govindaraju,** Department of Electronics and Communication Engineering for his consistent support throughout the course of this project work.

We are greatly privileged to express our deep sense of gratitude and heartfelt thanks to our Project Guide **Dr. A. Vasuki,** Department of Electronics and Communication Engineering for her expert counselling and guidance to make this project to a great deal of success and also we wish to convey our regards to all teaching and non-teaching staff of ECE Department for their help and cooperation.

Finally, we thank our parents and our family members for giving us the moral support and abundant blessings in all of our activities and our dear friends who helped us to endure our difficult times with their unfailing support and warm wishes.

ABSTRACT

There has been an ever-increasing interest on multi sensor-data fusion technology driven by its versatility and diverse areas of applications. Multi-sensor image fusion is the process of combining relevant information from two images into a single image which will be more informative than the input images. Several applications in satellite image processing require high spatial as well as high spectral resolution in a single image. However, capturing such images directly is not possible due to technical limitations. One possible solution for this is image fusion. The panchromatic image acquired by satellites is transmitted with high spatial resolution and the multispectral image is transmitted with high spectral resolution. At the receiver station, both the images are fused to give an image with high spectral and high spatial resolution.

Conventional image fusion methods such as high pass filtering, averaging, Brovey method, principal component analysis, discrete wavelet transform, and others suffer the disadvantage of producing spatial distortion in the fused image and also leading to spectral distortion when going in for further processing. The proposal is for a new pan-sharpening method named Sparse fusion of Images. The Sparse fusion algorithm gives a high spatial resolution and less spectral distortion compared to the other conventional methods. Thus this technique is proposed which does not assume any spectral composition model of the panchromatic image.

The Sparse Fusion algorithm is based on the compressive sensing theory and explores the sparse representation of Low Resolution multispectral image patches in the dictionary pairs constrained from the panchromatic image and its down-sampled low resolution version. The image is then reconstructed from the patches in the dictionary pairs. The Sparse Fusion algorithm is simulated using MATLAB and is to be implemented on a Field Programmable

Gate Array. The performance of the fused image is analysed using following parameters such as Root Mean Square Error (RMSE), Relative Global Dimensional Synthesis Error (ERGAS), Correlation Coefficient, Degree of Distortion and Q-average. The Sparse Fusion algorithm finds its applications in Remote Sensing, land-use classification, map updating and disaster management.

TABLE OF CONTENTS

LIST OF ABBREVIATIONS

LR	Low Resolution
HR	High Resolution
DWT	Discrete Wavelet Transform
PCA	Principal Component Analysis
IHS	Intensity-Hue-Saturation
RMSE	Root Mean Square Error
ERGAS	Errur Relative Globale Adimensionnelle de Synth*è*se
DD	Degree of Distortion
UIQI	Universal Image Quality Index
HDL	Hardware Description Language
XSG	Xilinx System Generator
SAM	Spectral Angle Mapper
FPGA	Field Programmable Logic Array
DSP	Digital Signal Processing
IC	Integrated Circuit
JTAG	Joint Tag Access Group
RTL	Register-Transfer Level
GUI	Graphical User Interface

LIST OF FIGURES

LIST OF TABLES

CHAPTER 1

INTRODUCTION

Image processing is a method to perform some operations on an image, in order to get an enhanced image or to extract some useful information from it. It is a type of signal processing in which input is an image and output may be image or characteristics/features associated with that image.There are two types of methods used for image processing namely, analogue and digital image processing. Analogue image processing can be used for the hard copies like printouts and photographs. Image analysts use various fundamentals of interpretation while using these visual techniques. Digital image processing techniques help in manipulation of the digital images by using computers.

Image fusion is the process of combining relevant information from two or more images into a single image. Pan-sharpening, a special form of image fusion used in satellite imagery, is a process of merging high-resolution panchromatic and low-resolution multispectral images to create a single high-resolution colour image. Google Maps and nearly every map creating company use this technique to increase image quality.

Satellite imagery consists of images of Earth or other planets collected by satellites. Satellite images have many applications in meteorology, oceanography, fishing, agriculture, biodiversity conservation, forestry, landscape, geology, cartography, regional planning, education, intelligence and warfare. Pan-sharpening plays a vital role in the field of satellite imagery and remote sensing because, the images transmitted from the various satellites around the earth are in the form of high resolution panchromatic images and low resolution multispectral images due to the constraints over the transmitting bandwidth. Hence the two images obtained over the same region are fused to obtain a multispectral image with a higher resolution which can be further used for many other applications. There are four types of resolutions in satellite

imagery in remote sensing: spatial, spectral, temporal, and radiometric. The resolution of satellite images varies depending on the instrument used and the altitude of the satellite's orbit.

A panchromatic image consists of only one band. It is usually displayed as a grey scale image, i.e. the displayed brightness of a particular pixel is proportional to the pixel digital number which is related to the intensity of solar radiation reflected by the targets in the pixel and detected by the detector. Thus, a panchromatic image may be similarly interpreted as a black-and-white aerial photograph of the area. The Radiometric Information is the main information type utilized in the interpretation.

A multispectral image is one that captures image data at specific frequencies across the electromagnetic spectrum. The wavelengths may be separated by filters or by the use of instruments that are sensitive to particular wavelengths, including light from frequencies beyond the visible light range, such as infrared. A multispectral image consists of several bands of data. For visual display, each band of the image may be displayed one band at a time as a grey scale image, or in combination of three bands at a time as a colour composite image. Interpretation of a multispectral colour composite image will require the knowledge of the spectral reflectance signature of the targets in the scene. In this case, the spectral information content of the image is utilized in the interpretation. Spectral imaging can allow extraction of additional information the human eye fails to capture with its receptors for red, green and blue. It was originally developed for space-based imaging. Multispectral images are the main type of images acquired by remote sensing radiometers. Dividing the spectrum into many bands, multispectral is the opposite of panchromatic, which records only the total intensity of radiation falling on each pixel. Usually, Earth observation satellites have three or more radiometers. Each acquires one digital image in a small spectral band.

Many remote sensing applications such as land-use classification, change detection, map updating, and hazard monitoring require images with both high

spectral and high spatial resolution (HR). However, due to technological limitations of current remote sensors, the data provided by most topographic Earth observation satellites such as IKONOS, quickbird, geoeye, and worldview-2 are composed of a panchromatic channel of HR and several (typically 3–8) multispectral channels at a lower spatial resolution (LR).

While the HR panchromatic image allows for accurate geometric analysis, the LR spectral channels provide the spectral information, necessary for thematic interpretation.

Simple pan-sharpening methods aim at providing a colour image of pleasing and sharp appearance. This is facilitated by the fact that the human visual perception has an LR in the three colour channels than in the black and white (panchromatic) channel. Quantitative evaluation of remote sensing data, however, calls for more sophisticated methods. The aim is obtaining an HR multispectral image as if it was acquired by a sensor with the same spectral response as the multispectral sensors but the spatial resolution of the panchromatic sensor. A particular difficulty is that, in general, the panchromatic pixel value cannot be considered to be simply the linear combination of the ones in the spectral bands. The reason is that the spectral bands may not add up to the panchromatic sensitivity band.

Due to the mentioned significant difference of the gray value between the panchromatic and multispectral images, caused by different wavelength ranges, the conventional methods may suffer from significant spectral distortion. The goal of this project is to explore a sparse signal representation of image patches to solve the pan-sharpening problem. The Sparse fusion algorithm also does not assume any spectral composition model of the panchromatic image and gives robust performance against spectral model errors. Due to the super-resolution capability and robustness of the used sparse reconstruction technique, these methods are expected to give higher spatial and spectral resolution with less spectral distortion compared with other existing methods. The proposed

algorithm is generally applicable to image fusion, including hyper-spectral image sharpening or spectral un-mixing.

The report discusses on the various topics related to the satellite image fusion. The second chapter discusses the basics of image fusion such as the various parameters involved in the image fusion process. It also discusses the various conventional methods available for the satellite image fusion, its advantages and drawbacks, performance and techniques.

The third chapter is the detailed explanation of the proposed Sparse fusion algorithm. It consists of the pre-requisites of the algorithm, flow chart, formulas and process of execution.

The fourth chapter tells about the various performance metrics available to measure the performance of the algorithm from the output images obtained. The indication of each metric, its default values, the formulas are discussed under this chapter.

The fifth chapter explains the MATLAB simulation of the Sparse fusion algorithm and also shows the results obtained for the various input image sets. It also shows a comparison between the proposed algorithm and Another conventional method, the Brovey Transform method depicting the robustness of the Sparse fusion algorithm over model errors.

The sixth chapter is about an initiative taken to implement the Sparse fusion algorithm over an FPGA using Xilinx System Generator and Converting the MATLAB code into VerilogHDL. The .v file runs on a Xilinx simulator and .bit file is generated to be downloaded on the FPGA.

CHAPTER 2
IMAGE FUSION

2.1 Introduction

Image fusion is a process of combining two or more images to enhance the information content. Image fusion techniques are important as it improves the performance of object recognition systems by integrating many sources of satellite, airborne and ground based imaging systems with other related datasets. Further, it also helps in sharpening the images, improve geometric corrections, enhance certain features that are not visible in either of the images, replace the defective data, complement the datasets for better decision making. It combines the significant information from two or more source images into a single resultant image that describes the scene better and retains useful information from the input images. Image fusion techniques are widely used in various applications such as remote sensing, medical imaging, military and astronomy.

A high resolution panchromatic image gives geometric details of an image because of the presence of natural as well as man-made objects in the scene and a low resolution multispectral image gives the colour information of the source image. The aim of multi-sensor image fusion is to represent the visual information from multiple images having different geometric representations into a single resultant image without any information loss. The advantages of image fusion include image sharpening, feature enhancement, improved classification, and creation of stereo datasets. Multi-sensor image fusion provides the benefits in terms of range of operation, spatial and temporal characteristics, system performance, reduced ambiguity and improved reliability.

Based on the processing levels, image fusion techniques can be divided into different categories. These are pixel level, feature level and symbol level decision level. Pixel level method is the simplest and widely used method. This method processes pixels in the source image and retains most of the original

image information. Compared to other two methods pixel level image fusion gives more accurate results. Feature level method processes the characteristics of the source image. This method can be used with the decision level method to fuse images effectively. Because of the reduced data size, it is easier to compress and transmit the data.

The top level of image fusion is decision making level. It uses the data information extracted from the pixel level fusion or the feature level fusion to make optimal decision to achieve a specific objective. Moreover, it reduces the redundancy and uncertain information.

2.2 Image Fusion Techniques

In the process of image fusion, the good information from each of the given images is fused together to form a resultant image whose quality is superior to any of the input images. Image fusion method can be broadly classified into two groups –

1. Spatial domain fusion method
2. Transform domain fusion method

Spatial domain techniques directly deal with the image pixels. The pixel values are manipulated to achieve desired result. In frequency domain methods the image is first transferred in to frequency domain. It means that the Fourier Transform of the image is computed first. All the Fusion operations are performed on the Fourier transform of the image and then the Inverse Fourier transform is performed to get the resultant image.

Image Fusion applied in every field where images are ought to be analyzed. For example, medical image analysis, microscopic imaging, analysis of images from satellite, remote sensing Application, computer vision, robotics etc. The fusion methods such as averaging, Brovey method, principal component analysis (PCA) and IHS based methods fall under spatial domain approaches. Another important spatial domain fusion method is the high pass filtering based technique. The disadvantage of spatial domain approaches is that

they produce spatial distortion in the fused image. Spectral distortion becomes a negative factor while we go for further processing such as classification problem. Spatial distortion can be very well handled by frequency domain approaches on image fusion.

The multi resolution analysis has become a very useful tool for analyzing remote sensing images. The discrete wavelet transform has become a very useful tool for fusion. Some other fusion methods are also there such as Laplacian-pyramid based, Curvelet transform based etc. These methods show a better performance in spatial and spectral quality of the fused image compared to other spatial methods of fusion.

There are various methods that have been developed to perform image fusion. Some well-known image fusion methods are listed below:-

(1) Intensity-hue-saturation (IHS) transform based fusion

(2) Principal component analysis (PCA) based fusion

(3) Multi scale transform based fusion:-

- (a) High-pass filtering method
- (b) Pyramid method:-
  - (i) Gaussian pyramid
  - (ii) Laplacian Pyramid
  - (iii) Gradient pyramid
  - (iv) Morphological pyramid
  - (v) Ratio of low pass pyramid
- (c) Wavelet transforms:-
  - (i) Discrete wavelet transforms (DWT)
  - (ii) Stationary wavelet transforms
  - (iii) Multi-wavelet transforms
- (d) Curvelet transforms

Due to the limited focus depth of the optical lens it is often not possible to get an image that contains all relevant objects in focus. To obtain an image with

every object in focus a multi-focus image fusion process is required to fuse the images giving a better view for human or machine perception. Some of the conventional algorithms are explained.

2.2.1 Simple Average

It is a well documented fact that regions of images that are in focus tend to be of higher pixel intensity. Thus this algorithm is a simple way of obtaining an output image with all regions in focus. The value of the pixel P (i, j) of each image is taken and added. This sum is then divided by 2 to obtain the average. The average value is assigned to the corresponding pixel of the output image which is given in equation (1). This is repeated for all pixel values.

$$K(i, j) = \{X(i, j) + Y(i, j)\}/2 \qquad (2.1)$$

where X (i , j) and Y (i, j) are two input images.

2.2.2 Select Maximum

The greater the pixel values the more in focus the image. Thus this algorithm chooses the in-focus regions from each input image by choosing the greatest value for each pixel, resulting in highly focused output. The value of the pixel P (i, j) of each image is taken and compared to each other. The greatest pixel value is assigned to the corresponding pixel.

2.2.3 Discrete Wavelet Transform (DWT)

Wavelets are finite duration oscillatory functions with zero average value. They have finite energy. They are suited for analysis of transient signal. The irregularity and good localization properties make them better basis for analysis of signals with discontinuities. Wavelets can be described by using two functions: the scaling function f (t), also known as “father wavelet” and the

wavelet function or “mother wavelet”. Mother wavelet (t) undergoes translation and scaling operations to give self similar wavelet families.

The wavelet transform decomposes the image into low-high, high-low, high-high spatial frequency bands at different scales and the low-low band at the coarsest scale. The L-L band contains the average image information whereas the other bands contain directional information due to spatial orientation. Higher absolute values of wavelet coefficients in the high bands correspond to salient features such as edges or lines.

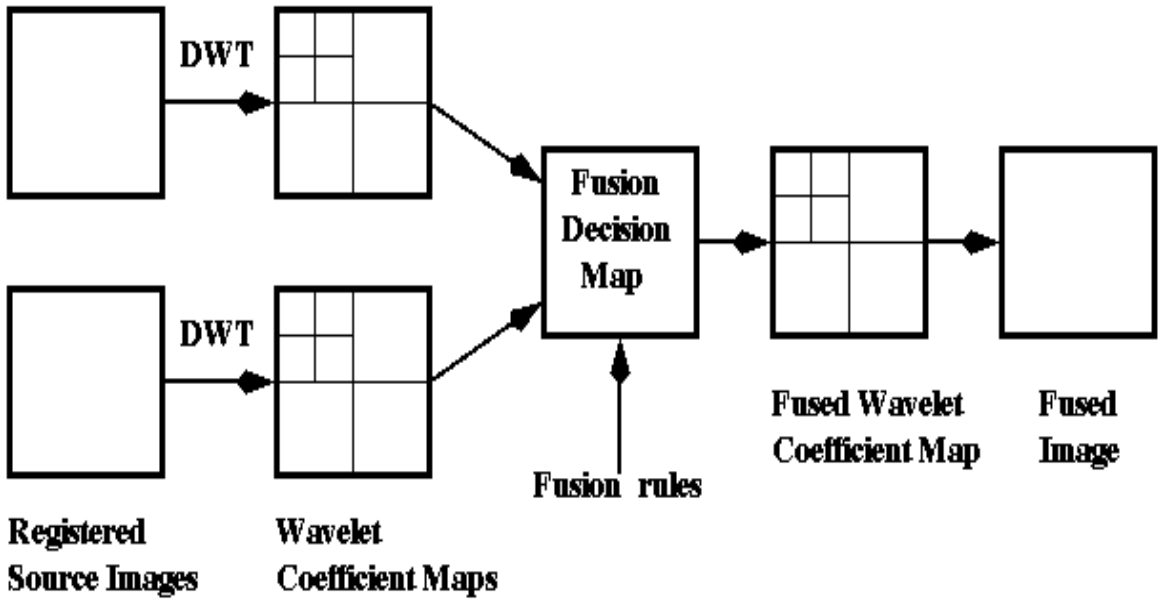

Fig 2.1 DWT Image Fusion Algorithm

2.2.4 Principal Component Analysis (PCA)

PCA is a mathematical tool which transforms a number of correlated variables into a number of uncorrelated variables. The PCA is used extensively in image compression and image classification. The PCA involves a mathematical procedure that transforms a number of correlated variables into a number of uncorrelated variables called principal components. It computes a compact and optimal description of the data set.

The first principal component accounts for as much of the variance in the data as possible and each succeeding component accounts for as much of the remaining variance as possible. First principal component is taken to be along the direction with the maximum variance. The second principal component is constrained to lie in the subspace perpendicular of the first. Within this subspace, this component points the direction of maximum variance. The third principal component is taken in the maximum variance direction in the subspace perpendicular to the first two and so on.

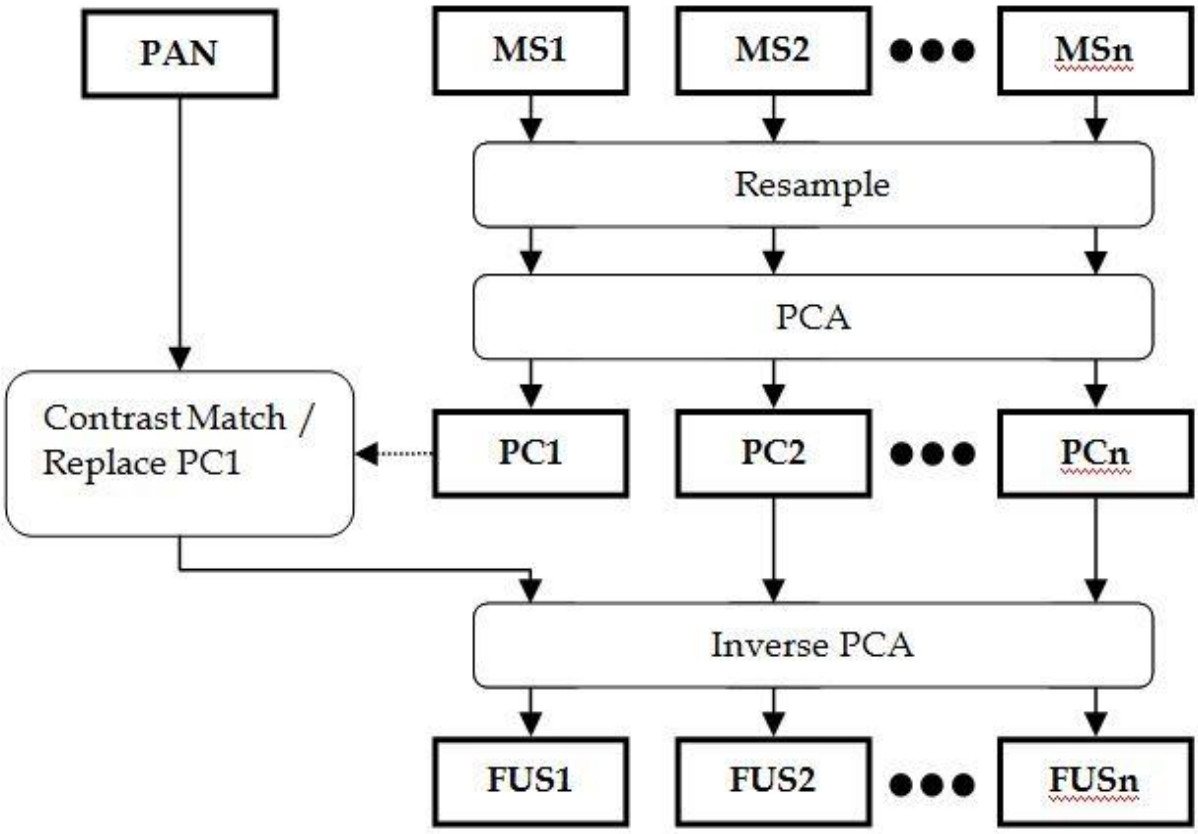

Fig 2.2 PCA Image Fusion Algorithm

Pan-sharpening can be referred to as a special case of image fusion. Research in the image fusion area is mostly focused on improving fusion quality and reducing colour distortion. Among the existing hundreds of various pan-

sharpening methods, the most popular ones are intensity–hue–saturation technique (IHS), principal component analysis (PCA), Brovey transform, and wavelet-based fusion. Due to significant difference of the gray value between the panchromatic and multispectral images, caused by different wavelength ranges, the conventional methods may suffer from significant spectral distortion. The Sparse fusion algorithm holds strong because it does not consider the spectral properties during the fusion process.

CHAPTER 3

SPARSE FUSION ALGORITHM

Pan-sharpening requires a low-resolution (LR) multispectral image **Y** with *N* channels and a high-resolution (HR) panchromatic image **X**0 and aims at increasing the spatial resolution of **Y** while keeping its spectral information, i.e., generating an HR multispectral image **X** utilizing both **Y** and **X**0 as inputs. The Sparse fusion algorithm reconstructs the HR multispectral image in an efficient way by ensuring both high spatial and spectral resolution with less spectral distortion. It consists of three main steps:

1) Dictionary learning.

2) Sparse coefficients estimation.

3) HR multispectral image reconstruction.

3.1 Dictionary Learning

The HR pan image **X**0 is low-pass filtered and down-sampled by a factor of *F*DS (typically 4–10) such that it has a final point spread function similar to a sampling grid identical to the multispectral channels. The resulting LR version of **X**0 is called **Y**0. This down-sampling step may be combined with the co-registration of the different channels. The LR pan image **Y**0 and the LR multispectral image **Y** are tiled into small, partially overlapping patches **y**0 and **y***k*, where *k* stands for the *k*th channel and $k = 1, \ldots, N$. All the LR patches **y**0 with pixel values arranged in column vectors form the matrix **D***l* called the LR dictionary. Likewise, the HR dictionary **D***h* is generated by tiling the HR pan image **X**0 into patches **x**0 of *F*DS times the size as the LR pan image patches, such that each HR patch corresponds to an LR patch. These image patches are called “atoms” of the dictionaries. Fig. 4.1 provides an example of a few corresponding LR and HR atoms from the dictionary pair **D***h* and **D***l*.

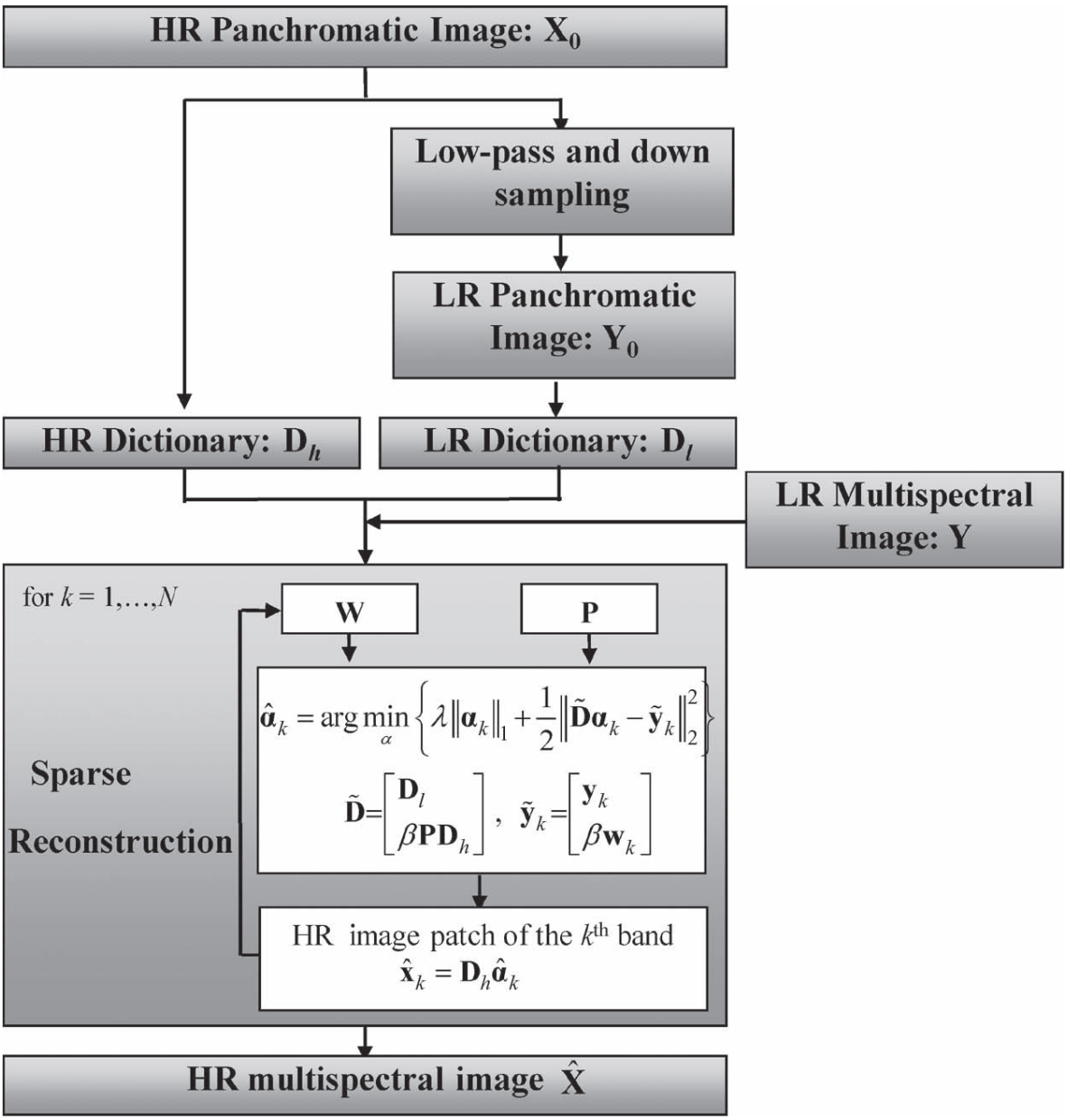

Fig 3.2 Flow Chart Of Sparse Fusion

In this method, the dictionary pair is learnt directly from the image itself. Due to the fact that the dictionaries are built up from the pan image observing the same area and acquired at the same time as the multispectral channels, the LR multispectral image patches **y***k* and their corresponding HR patches **x***k* to be reconstructed are expected to have a sparse representation in this LR/HR dictionary pair. Furthermore, the corresponding **y***k* and **x***k* share the same sparse coefficients in **D***h* and **D***l*. This gives us an alternative method for image fusion when large collections of representative satellite images are not available.

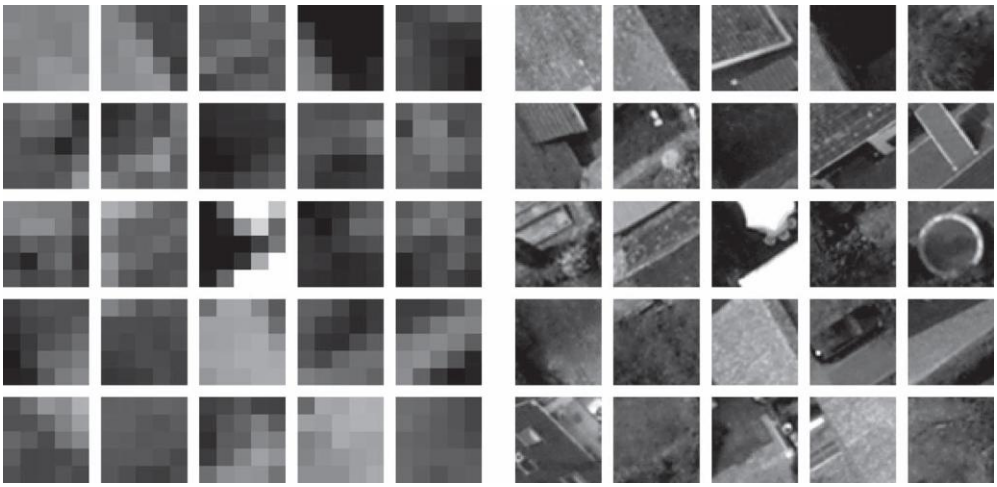

Fig 3.1 Sample Dictionary image

3.2 Sparse Coefficients Estimation

This step attempts to represent each LR multispectral patch in the *k*th channel **y***k* as a linear combination of LR pan patches **y**0, i.e., of the atoms of the dictionary **D***l* with a coefficient vector denoted by $\hat{\boldsymbol{\alpha}}k$. Since this dictionary is over-complete, i.e., its columns are not orthogonal, there may be infinitely many solutions. The "best" solution is the one employing the least number of pan patches. Therefore, for each LR multispectral patch **y***k*, a sparse coefficient vector $\hat{\boldsymbol{\alpha}}k$. is estimated by an $L1 - L2$ minimization:

$$\hat{\alpha}_k = \arg\min_{\alpha}\left\{\lambda\left\|\alpha_k\right\|_1 + \frac{1}{2}\left\|\hat{D}_{\alpha_k} - \hat{y}_k\right\|_2^2\right\} \qquad (3.1)$$

Where,

$$\hat{D} = \begin{bmatrix} D_l \\ \beta P D_h \end{bmatrix} \qquad \hat{y}_k = \begin{bmatrix} y_k \\ \beta w_k \end{bmatrix} \qquad (3.2)$$

Matrix **P** is a matrix that extracts the region of overlap between the current target patch and previously reconstructed ones. **W***k* contains the pixel values of the previously reconstructed HR multispectral image patch on the overlap region. If the patches do not overlap, $\widetilde{\mathbf{D}}$ = **D***l* and $\tilde{y}k$ = **y***k*. Parameter β is a weighting factor that gives a trade-off between goodness of fit of the LR input and the consistency of reconstructed adjacent HR patches in the overlapping

area; β is chosen to be $1/F2$ DS, i.e., we weight the overlapped and non overlapped areas according to their physical sizes. λ is the standard Lagrangian multiplier, balancing the sparsity of the solution and the fidelity of the approximation to $\mathbf{y}k$. If and only if the dictionaries are stable, solving (1) by means of standard convex optimization algorithms can give the sparsest solution, though with systematic amplitude bias introduced by the $L1$-norm approximation of the NP hard $L0$-norm minimization problem. However, due to the fact that the atoms in the dictionaries are often highly coherent, the dictionaries are normally not stable. Hence, we estimate the sparse coefficient $\hat{\boldsymbol{\alpha}}k$.

3.3 HR Multispectral Image Reconstruction:

Since each of the HR image patches $\mathbf{x}k$ is assumed to share the same sparse coefficients as the corresponding LR image patch $\mathbf{y}k$ in the coupled HR/LR dictionary pair, i.e., the coefficients of $\mathbf{x}k$ in $\mathbf{D}h$ are identical to the coefficients of $\mathbf{y}k$ in $\mathbf{D}l$, the final sharpened multispectral image patches $\mathbf{x}k$ are reconstructed by

$$\hat{\boldsymbol{X}}\mathrm{k} = \mathbf{D}h\,\hat{\boldsymbol{\alpha}}k. \qquad (3.3)$$

The tiling and summation of all patches in all individual channels finally give the desired pan-sharpened image $\hat{\boldsymbol{X}}$. The proposed Sparse fusion algorithm is supposed to demonstrate the potential of sparse signal reconstruction for data fusion.

CHAPTER 4

PERFORMANCE METRICS

The performance of the fusion algorithm can be analysed using the following parameters:

4.1 RMSE

The RMSE is frequently used to compare the difference between the original and pan-sharpened images by directly calculating the changes in pixel values. It is defined as

$$RMSE = \sqrt{\frac{1}{MN}\sum_{i=1}^{M}\sum_{j=1}^{N}(X_{i,j} - \hat{X}_{i,j})^2} \qquad (4.1)$$

Xi,j is the pixel value of the original image **X**, and $\widehat{\boldsymbol{X}}i,j$ is the pixel value of the pan-sharpened image $\widehat{\boldsymbol{X}}$. *M* and *N* are the HR image sizes. The pan-sharpened image is closer to the original image when RMSE is smaller.

4.2 UIQI (Q-average)

The UIQI has been widely used to assess the quality of image sharpening recently. It is defined as

$$Q_0 = \frac{\sigma_{x\hat{x}}}{\sigma_x.\sigma_{\hat{x}}} \cdot \frac{2\bar{x}\bar{\hat{x}}}{\left(\bar{x}^2 + \bar{\hat{x}}^2\right)} \cdot \frac{2\sigma_x\sigma_{\hat{x}}}{\left(\sigma_x{}^2 + \sigma_{\hat{x}}{}^2\right)} \qquad (4.2)$$

where *x*, *σx* and ˆ*x*, *σ*ˆ*x* are the mean values and standard deviations of the original image **X** and the pan-sharpened image $\widehat{\boldsymbol{X}}$, respectively. It combines three different factors, namely, loss of correlation, luminance distortion, and contrast distortion. The best value of Q-average is 1.

4.3 ERGAS

The ERGAS reflects the overall quality of the pan-sharpened image. It represents the difference between the pan-sharpened and original images and is defined as

$$ERGAS = 100\frac{h}{l}\sqrt{\frac{1}{k}\sum_{k=1}^{K}\left[\frac{RMSE_k}{\bar{\hat{X}}_k}\right]^2} \tag{4.3}$$

where *h/l* is the ratio between pixel sizes of the panchromatic and original multispectral images, and RMSE*k* and $\widehat{\boldsymbol{X}}k$ are the RMSE and mean values of the *k*th band, respectively. A small ERGAS value means small spectral distortion so that the algorithm has high preservation of spectral information.

4.4 Degree of Distortion: The degree of distortion directly reflects the level of pan-sharpened image distortion. It is defined as

$$D = \frac{1}{MN}\sum_{i=1}^{M}\sum_{j=1}^{N}\left|X_{i,j} - \hat{X}_{i,j}\right| \tag{4.4}$$

The distortion of the pan-sharpened image is small, whereas the value of *D* is small.

4.5 Correlation Coefficient (ρ):

The correlation coefficient of the pan-sharpened and original images measures the similarity of spectral feature. It is defined as

$$\rho = \frac{\sum_{i,j}\left[(X_{i,j} - \bar{x}).(\hat{X}_{i,j} - \bar{\hat{x}})\right]}{\sqrt{\sum_{i,j}\left[(X_{i,j} - \bar{x})^2\right]\sum_{i,j}\left[\left(\hat{X}_{i,j} - \bar{\hat{x}}\right)^2\right]}} \tag{4.5}$$

where *x* and $\widehat{\boldsymbol{x}}$ are the mean values of the original image **X** and the pan-sharpened image $\widehat{\boldsymbol{X}}$, respectively. A correlation coefficient of close to +1 means that the two images are highly correlated.

CHAPTER 5

SIMULATION OF SPARSE FUSION

5.1 Introduction

The Sparse fusion algorithm is simulated using MATLAB software over various image sets of high resolution panchromatic and low resolution multispectral images. The fused multispectral image is obtained with a higher resolution than the input multispectral image. From this very HR multispectral image, we simulate the panchromatic image X0 by linearly combining the multispectral bands and adding some model error

$$X0 = c1X1 + c2X2 + c3X3 + c4X4 + \varepsilon \qquad (5.1)$$

Xk and ck are the values of the kth band of the HR multispectral image, and its corresponding weighting coefficient. E is the model error. A simulated LR multispectral image Y is obtained by low-pass filtering and down-sampling the original image, i.e., the HR multispectral image X. As a validation, we use the proposed method to reconstruct the HR multispectral image $\hat{X}$. By comparing to the original multispectral image X, we access its performance with respect to conventional methods.

To investigate the robustness of the algorithm against model errors, the panchromatic image with a reasonable model error is simulated. The corresponding LR multispectral image obtained by downsampling the HR multispectral image. From the two input images, the HR multispectral image can be reconstructed and then be compared with the original HR multispectral image. The HR multispectral image reconstructed using the proposed Sparse fusion method and Brovey transform method. Compared with the results produced by conventional pan-sharpening method, Brovey transform, it is verified that Sparse fusion can produce better results.

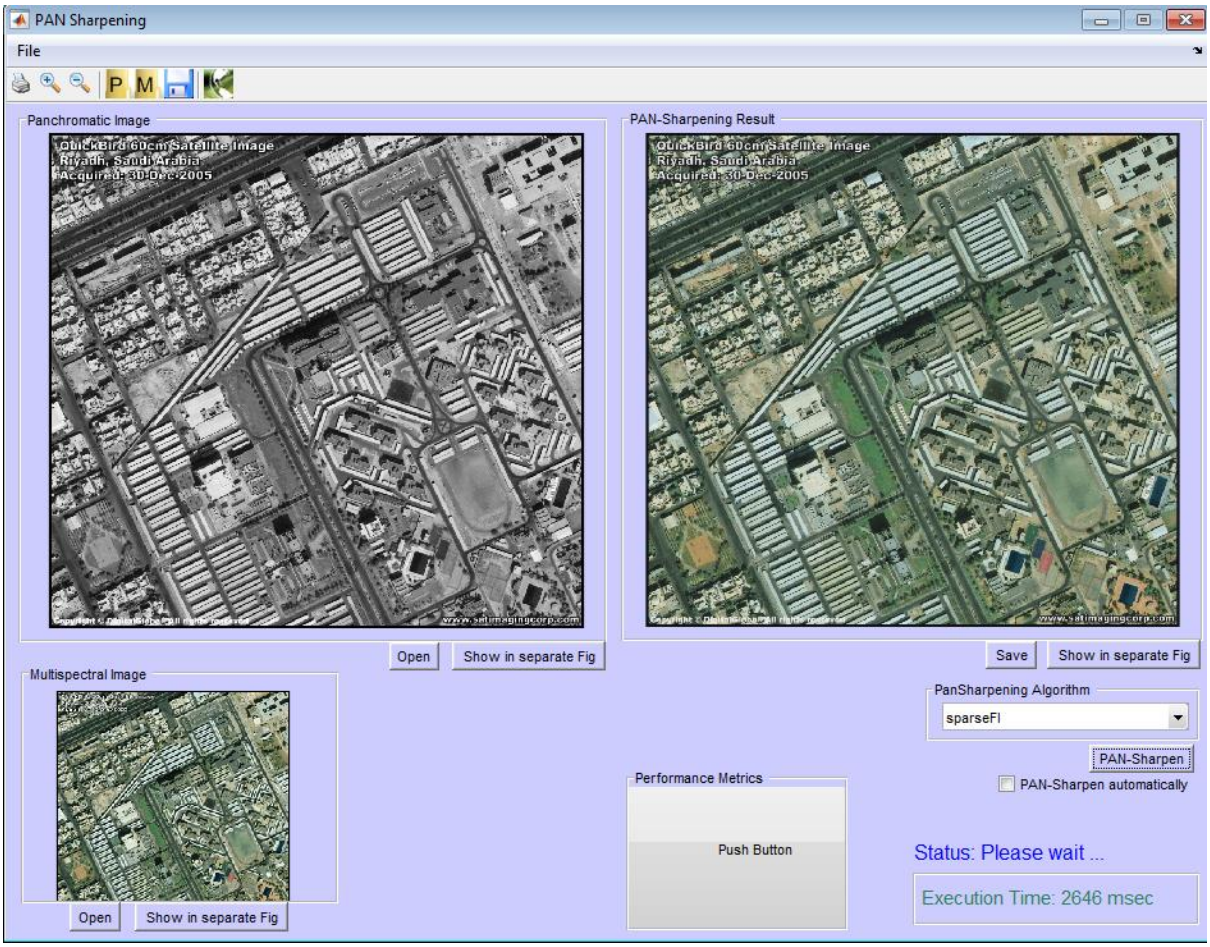

Fig 5.1 MATLAB GUI Window

The MATLAB simulation GUI window appears as shown in Fig 5.1. The pop-up window is developed by using the Graphical User Interface function available in the MATLAB. The window serves easy for selecting the input images and the output is obtained over a button click. It also contains the drop down menu for selecting whether Brovey or Sparse fusion method. There are options for displaying the images as separate figures too.

5.2 Simulation Results

Simulation result 1 - Copacabana Beach - GeoEye1.

The Sparse fusion is performed for a HR panchromatic image and a LR multispectral image obtained from GeoEye1 satellite.

Fig 5.2 HR Panchromatic Image 1 (763x763)

Fig 5.3 LR Multispectral Image 1 (256x256)

Fig 5.4 HR Multispectral Fused Image 1 (763x763)

Table 5.1

Performance Comparison of Set 1

	RMSE	ρ	D	UIQI	ERGAS
Brovey	15.4408	0.2718	7.3051	0.42491	5.6441
Sparse Fusion	**6.0741**	**0.9832**	**5.1059**	**0.73859**	**2.6789**
Optimum Values	0	1	0	1	0

The fused HR image is obtained, which is more informative than the LR multispectral image. The comparitive results (Table 5.1) are also obtained with the Brovey method. The proposed algorithm has shown better results compared to the Brovey method.

Simulation result 2 - Disneyland, Tokyo, Japan - GeoEye.

The Sparse fusion is performed for a HR panchromatic image and a LR multispectral image obtained from GeoEye1, over Disneyland, Tokyo, Japan. The fused HR image is obtained, which is more informative than the LR multispectral image.

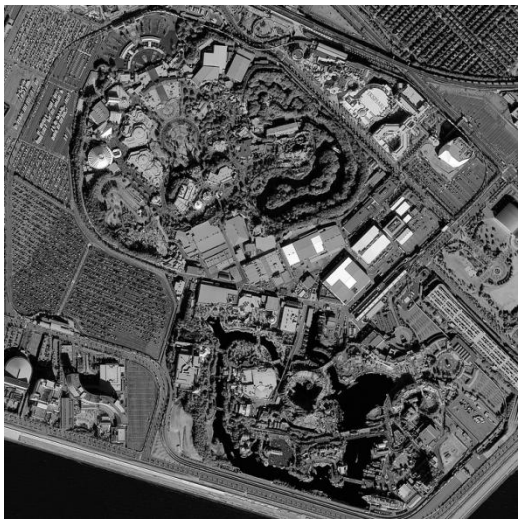

Fig 5.5 HR Panchromatic Image 2 (763x763)

Fig 5.6 LR Multispectral Image 2 (256x256)

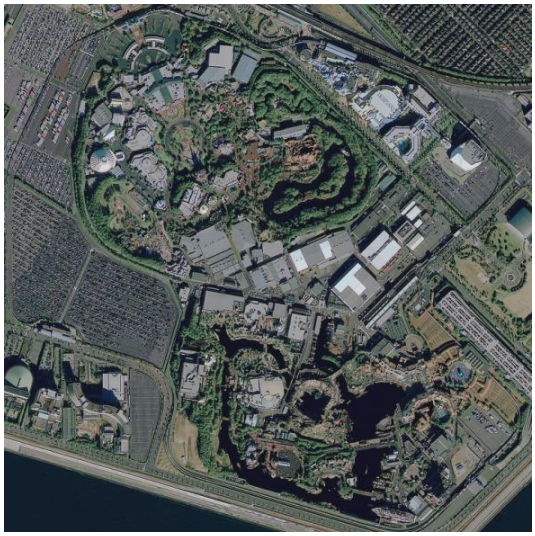

Fig 5.7 HR Multispectral Fused Image 2

(763x763)

Table 5.2

Performance Comparison of Set 2

	RMSE	ρ	D	UIQI	ERGAS
Brovey	15.4395	0.2778	7.2810	0.42493	5.6436
Sparse Fusion	**6.0690**	**0.9886**	**5.0957**	**0.73881**	**2.6767**
Optimum Values	0	1	0	1	0

The fused HR image is obtained, which is more informative than the LR multispectral image.The comparitive results (Table 5.2) show that Sparse fusion method is robust to model errors than Brovey method. The Sparse fusion method has shown parameters very close to the optimum values.

Simulation result 3 - Olympic Stadium, London - GeoEye1.

The Sparse fusion is performed for a HR panchromatic image and a LR multispectral image obtained from GeoEye1, over Olympic Stadium, London. A more informative HR multispectral image is obtained.

Fig 5.8 HR Panchromatic Image 3 (763x763)

Fig 5.9 LR Multispectral Image 3 (256x256)

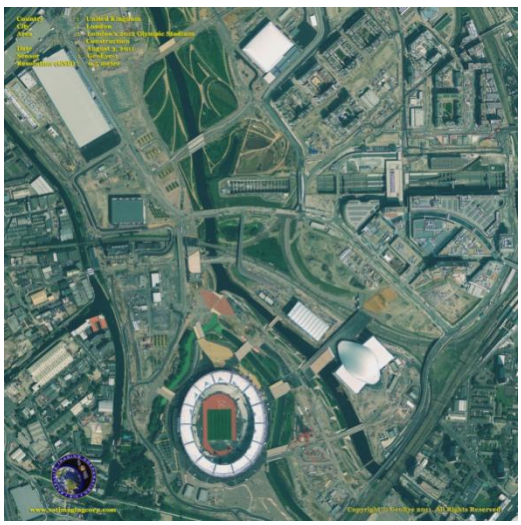

Fig 5.10 HR Multispectral Fused Image 3 (763x763)

Table 5.3

Performance Comparison of Set 3

	RMSE	ρ	D	UIQI	ERGAS
Brovey	15.4487	0.2759	7.2308	0.42429	5.6470
Sparse Fusion	**6.0746**	**0.9841**	**5.1303**	**0.74048**	**2.6791**
Optimum Values	0	1	0	1	0

Table 5.3 shows that the output obtained from the Sparse fusion method has shown better performance compared to the Brovey method. This depicts the robustness of the algorithm for errors over various conventional methods.

Simulation result 4 - Falirocoast, Athens, Greece - Ikonos.

The Sparse fusion is performed for a HR panchromatic image and a LR multispectral image obtained from IKONOS, over Falirocoast, Athens, Greece.

Fig 5.11 HR Panchromatic Image 4 (763x763)

Fig 5.12 LR Multispectral Image 4 (256x256)

Fig 5.13 HR Multispectral Fused Image 4

(763x763)

Table 5.4

Performance Comparison of Set 4

	RMSE	ρ	D	UIQI	ERGAS
Brovey	15.4451	0.2745	7.2923	0.42478	5.6456
Sparse Fusion	**6.0751**	**0.9849**	**5.1147**	**0.73878**	**2.6794**
Optimum Values	0	1	0	1	0

A more informative high resolution multispectral image is obtained from the input image set. Table 5.4 shows that the output obtained from the Sparse fusion method has shown better performance compared to the Brovey method. This depicts the robustness of the algorithm for errors over various conventional methods.

Simulation result 5 - Hungary, Europe - Ikonos.

The Sparse fusion is performed for a HR panchromatic image and a LR multispectral image obtained from IKONOS, over Hungary, Europe. On fusion, a HR multispectral image is obtained.

Fig 5.14 HR Panchromatic Image 5 (1024x1024)

Fig 5.15 LR Multispectral Image 5 (256x256)

Fig 5.16 HR Multispectral Fused Image 5 (1024x1024)

Table 5.5

Performance Comparison of Set 5

	RMSE	ρ	D	UIQI	ERGAS
Brovey	15.4406	0.2719	7.1774	0.42116	5.6440
Sparse Fusion	**6.0692**	**0.9899**	**5.1155**	**0.73957**	**2.6767**
Optimum Values	0	1	0	1	0

The fused HR image is obtained, which is more informative than the LR multispectral image. The comparitive results (Table 5.5) are also obtained with the Brovey method. The proposed algorithm has shown better results compared to the Brovey method.

Simulation result 6 - Barcelona, Spain - Ikonos.

The Sparse fusion is performed for a HR panchromatic image and a LR multispectral image obtained from IKONOS, over Barcelona, Spain. The fused HR image is obtained, which is more informative than the LR multispectral image.

Fig 5.17 HR Panchromatic Image 6 (1024x1024)

Fig 5.18 LR Multispectral Image 6 (256x256)

Fig 5.19 HR Multispectral Fused Image 6

(1024x1024)

Table 5.6

Performance Comparison of Set 6

	RMSE	ρ	D	UIQI	ERGAS
Brovey	15.4504	0.2730	7.2760	0.42453	5.6476
Sparse Fusion	**6.0683**	**0.9926**	**5.1057**	**0.73822**	**2.6763**
Optimum Values	0	1	0	1	0

On observing the Table 5.6, it is found that the Sparse fusion algorithm has shown better results over the Brovey method. the correlation coefficient is almost equal to the optimum value in the case of the Sparse fusion method whereas it is not the case in the Brovey method.

Simulation result 7 - Jinhua, China - QuickBird.

The Sparse fusion is performed for a HR panchromatic image and a LR multispectral image obtained from QuickBird, over Jinhua, China.

Fig 5.20 HR Panchromatic Image 7 (1024x1024)

Fig 5.21 LR Multispectral Image 7 (256x256)

Fig 5.22 HR Multispectral Fused Image 7 (1024x1024)

Table 5.7

Performance Comparison of Set 7

	RMSE	P	D	UIQI	ERGAS
Brovey	15.4476	0.2751	7.3083	0.42501	5.6466
Sparse Fusion	**6.0680**	**0.9869**	**5.0817**	**0.73864**	**2.6762**
Optimum Values	0	1	0	1	0

Table 5.7 shows that the output obtained from the Sparse fusion method has shown better performance compared to the Brovey method. This depicts the robustness of the algorithm for errors over various conventional methods.

Simulation result 8 - Boardwalk, Atlantic City, USA - QuickBird.

The Sparse fusion is performed for a HR panchromatic image and a LR multispectral image obtained from QuickBird, over Boardwalk, Atlantic City, USA. The fused HR image is obtained, which is more informative than the LR multispectral image.

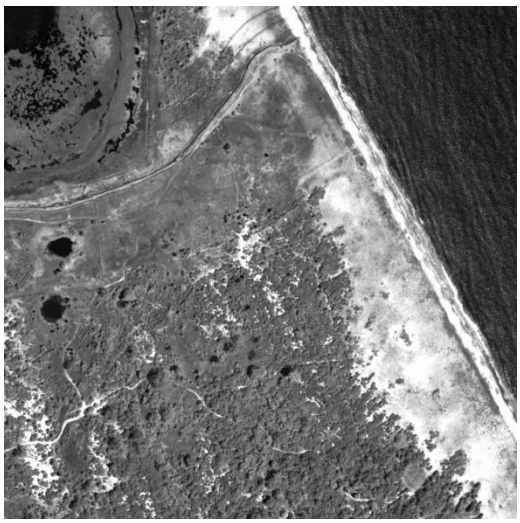

Fig 5.23 HR Panchromatic Image 8 (1024x1024)

Fig 5.24 LR Multispectral Image 8 (256x256)

Fig 5.25 HR Multispectral Fused Image 8

(1024x1024)

Table 5.8

Performance Comparison of Set 8

	RMSE	ρ	D	UIQI	ERGAS
Brovey	15.4336	0.2756	7.1861	0.42456	5.6414
Sparse Fusion	**6.0707**	**0.9887**	**5.1137**	**0.73909**	**2.6774**
Optimum Values	0	1	0	1	0

A more informative high resolution multispectral image is obtained from the input image set. Table 5.8 shows that the output obtained from the Sparse fusion method has shown better performance compared to the Brovey method. This depicts the robustness of the algorithm for errors over various conventional methods.

Simulation result 9 - Sydney, Australia, QuickBird.

The Sparse fusion is performed for a HR panchromatic image and a LR multispectral image obtained from QuickBird, over Sydney, Australia. The fused HR image is obtained, which is more informative than the LR multispectral image.

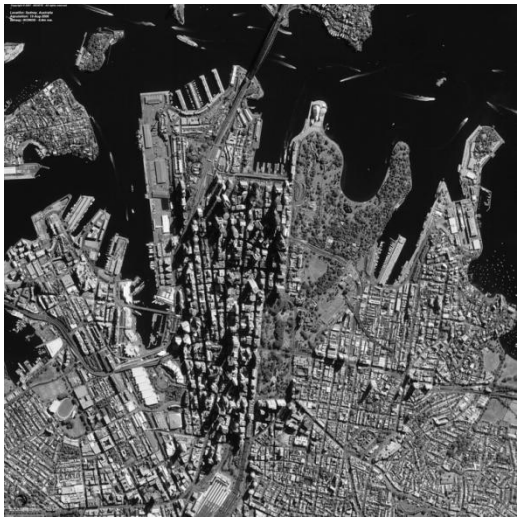

Fig 5.26 HR Panchromatic Image 9 (763x763)

Fig 5.27 LR Multispectral Image 9 (256x256)

Fig 5.28 HR Multispectral Fused Image 9 (763x763)

Table 5.9

Performance Comparison of Set 9

	RMSE	ρ	D	UIQI	ERGAS
Brovey	15.4477	0.2745	7.2414	0.42430	5.6466
Sparse Fusion	**6.0762**	**0.9816**	**5.1050**	**0.73869**	**2.6798**
Optimum Values	0	1	0	1	0

The fused HR image is obtained, which is more informative than the LR multispectral image. The comparitive results (Table 5.9) are also obtained with the Brovey method. The proposed algorithm has shown better results compared to the Brovey method.

Simulation result 10 - Palm Island, Dubai - QuickBird.

The Sparse fusion is performed for a HR panchromatic image and a LR multispectral image obtained from QuickBird, over Palm Island, Dubai. The fused HR image is obtained, which is more informative than the LR multispectral image.

Fig 5.29 HR Panchromatic Image 10 (5753x5643)

Fig 5.30 LR Multispectral Image 10 (256x256)

Fig 5.31 HR Multispectral Fused Image 10

(5753x5643)

Table 5.10

Performance Comparison of Set 10

	RMSE	ρ	D	UIQI	ERGAS
Brovey	15.4343	0.2744	7.3114	0.42543	5.6417
Sparse Fusion	**6.0769**	**0.9796**	**5.0891**	**0.73762**	**2.6801**
Optimum Values	0	1	0	1	0

Table 5.10 shows that the output obtained from the Sparse fusion method has shown better performance compared to the Brovey method. This depicts the robustness of the algorithm for errors over various conventional methods.

CHAPTER 6

HARDWARE IMPLEMENTATION

Field Programmable Gate Array (FPGA) is a reconfigurable IC. The implementation process of image fusion algorithms on hardware has the most viable solution for improving the performance of the systems. A Field Programmable Gate Array (FPGA) is one such reconfigurable hardware, offering superior features than DSP & other hardware device due to their product reliability & maintainability advantages in digital image processing. The multiple processing data sets require in many algorithms have to be performed sequentially on a computer and fused one pass in FPGA.

To create an FPGA design, using Hardware Description Language (HDL) such as VHDL or Verilog. Xilinx System Generator (XSG) is a MATLAB-Simulink based design tool which offers high performance. XSG for FPGA is a tool which offers block libraries that plugs into Simulink model tool is integrated with MATLAB window. Simulink has become an important part of engineering programs and industries. To start with Simulink in MATLAB, double-click on Simulink icon. The Simulink window opens. Then with the help of Simulink Library Browser, we can access the different toolboxes available for processing. The Video and Image processing block set contains a number of elements such as sources, sinks, math operators, parameters etc. The Xilinx Block set contains various elements shown below such as Basic Elements, Math, Shared Memory, Control logic, tools etc.

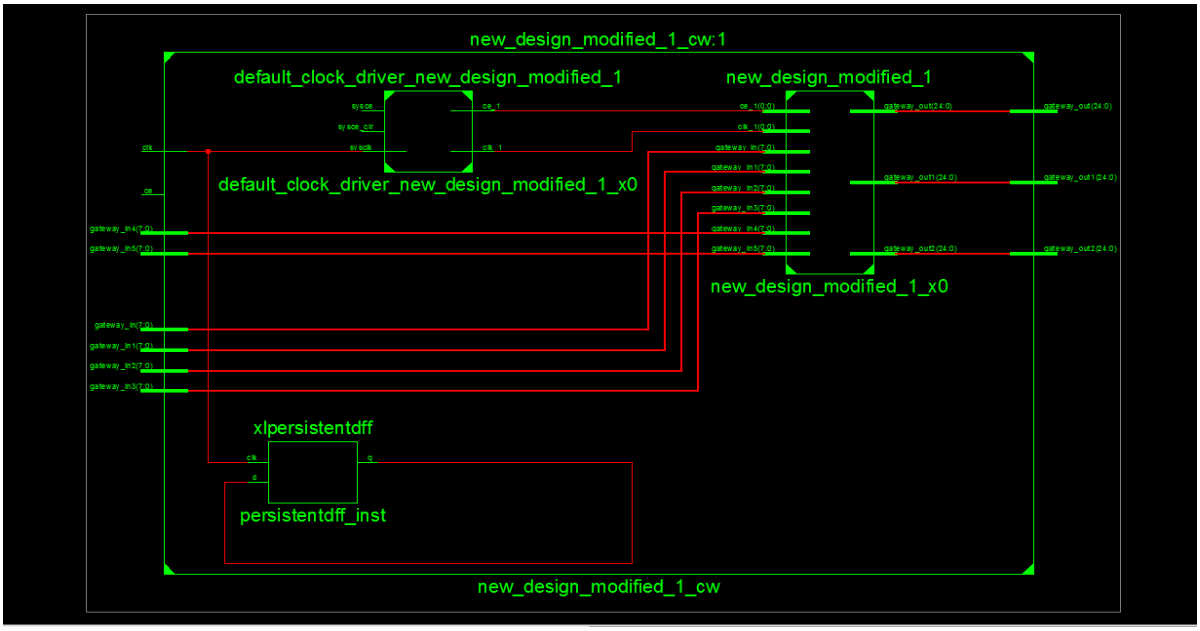

Fig 6.1 RTL schematic

Device Utilization Summary (estimated values)			[-]
Logic Utilization	**Used**	**Available**	**Utilization**
Number of Slice Registers	1	393600	0%
Number of fully used LUT-FF pairs	0	1	0%
Number of bonded IOBs	124	600	20%
Number of BUFG/BUFGCTRLs	1	32	3%

Fig 6.2 Device Utilization Summary

After obtaining the results, system generator is configured with FPGA board. Then, the programming file in VerilogHDL is created and can be accessed using Xilinx ISE. The simulation is now performed using Xilinx ISE suite and the output image is obtained as a bit stream. Later, hardware co-simulation block is generated. Hardware co-simulation block is used to perform hardware co-simulation using JTAG. To synthesis these modules net list files which serve as the input to the implementation module are created. After generating these files, the logic design is converted into a .bit file that can be downloaded on the FPGA.

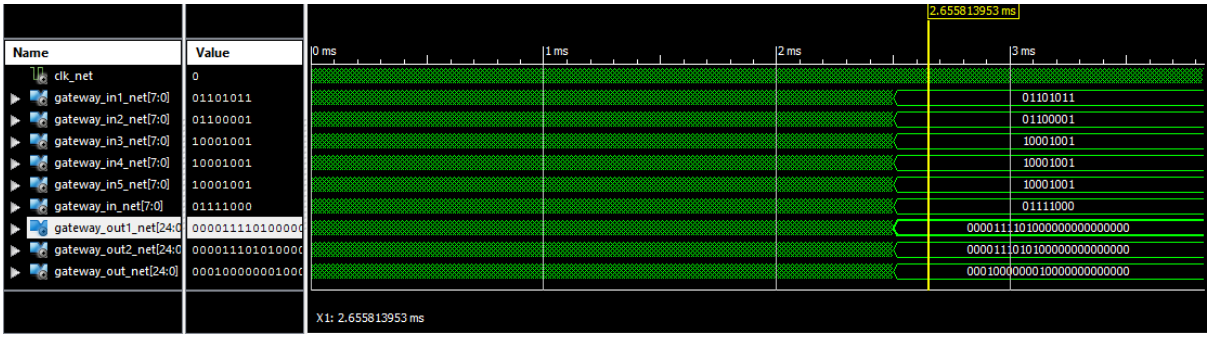

Fig 6.3 Xilinx simulation output

The .bit file is downloaded on the FPGA and it is run to obtain the results. The output image is viewed on a monitor using Visual Basic. As an initiative of the hardware implementation of the Sparse fusion algorithm, a simple averaging process of the fusion algorithm is implemented in an FPGA by building a relevant Simulink model and converting it into a Verilog code with the help of the system generator tool. The Xilinx simulation of the same is obtained.

CHAPTER 7
CONCLUSION

Many research papers have reported the limitations of existing fusion techniques. The most significant problems are spectral distortion, operator's fusion experience, the data set being fused, capacity of satellite sensor to store image data, etc. The satellites used from past decades are allocated the frequency band of visible spectrum region. Today, with increase in number of satellites launched by different nations, newer satellites are being assigned frequency bands of near infra-red region. This makes quality difference in imagery captured by older satellites and newer satellites. Hence, image fusion techniques give different results for imagery of newer satellites and old satellites. It is observed that, when traditional fusion and adjustment techniques are used with this imagery, captured by newer satellites, spectral distortion becomes a significant problem.

Hence, Sparse Fusion method will be a new technique in the field of Image fusion. The Sparse Fusion Technique does not assume any spectral composition model of the panchromatic image and due to the super-resolution capability and robustness of sparse signal reconstruction algorithm, it gives higher spatial resolution and less spectral distortion.

REFERENCES

1. Xiao Xiang Zhu and Richard Bamler, "A Sparse Image Fusion Algorithm with Application to Pan-Sharpening," IEEE transactions on geoscience and remote sensing, vol. 51, no. 5, may 2013.

2. C. Pohl and J. L. Van Genderen, “Multisensor image fusion in remote sensing: Concepts, methods and applications,” *Int. J. Remote Sens.*, vol. 19, no. 5, pp. 823–854, Mar. 1998.

3. S. Li and B. Yang, “A new pan-sharpening method using a compressed sensing technique,” *IEEE Trans. Geosci. Remote Sens.*, vol. 49, no. 2, pp. 738–746, Feb. 2011.

4. S. J. Wright, “Sparse optimization,” in *Proc. SIAM Conf. Optim.*, Darmstadt, Germany, May 2011.

5. K. Anil Kumar and M. Vijay Kumar, “Implementation of Image processing Lab using Xilinx System Generator”, Advances in Image and Video Processing, ISSN:2054-7412, vol.2, Issue 5, Sept 2014.

6. H. Li, B.S. Manjunath and S.K. Mitra, “ Multisensor image fusion using the wavelet transformation”, Graph Models Image Process. Vol.57, pp.235-245, 1995.

7. Laure.J.Chipman, Timothy M.Orr, Lewisn.Graham, “Wavelet and Image Fusion”, 1995 IEEE, Jan 2010, pp-248-249.

8. P. Phanindra, J. Chinnababu, V.Usha Shree, “FPGA Implementation of Medical Image Fusion based on DWT”, ISSN:2272-128x, vol.3, issues 9, sep-2013, pp-118-122.

9. Y. Zhang, “Problems in the fusion of commercial high-resolution satellite images as well as Landsat-7 images and initial solutions,” in Proc. Int. Archives Photogram. Remote Sens. Spatial Inf. Sci., 2002, vol. 34, pp. 587–592, Part 4.

10. D. Donoho, “Compressed sensing,” IEEE Trans. Inf. Theory, vol. 52, no. 4, pp. 1289–1306, Apr. 2006.

11. X. Zhu, X. Wang, and R. Bamler, “Compressive sensing for image fusion—With application to pan-sharpening,” in Proc. IGARSS Conf., 2011, pp. 2793–2796.

12. L. Alparone, L. Wald, J. Chanussot, C. Thomas, P. Gamba, and L. M. Bruce, “Comparison of pansharpening algorithms: Outcome of the 2006 GRS-S data-fusion contest,” IEEE Trans. Geosci. Remote Sens., vol. 45, no. 10, pp. 3012–3021, Oct. 2007

13. E. Candès, “Compressive sampling,” in Proc. Int. Congr. Math., Madrid, Spain, 2006, pp. 1433–1452.

14. X. Wang, “Compressive sensing for pan-sharpening,” M.S. thesis, Tech. Univ. Munich, Munich, Germany, 2011.

15. Strait, M., Rahmani, S., Markurjev, D., 2008, “Evaluation of Pan-Sharpening Methods, Research Experiences for Undergraduates”, (REU2008).

16. Wald, L., Ranchin, Th., Mangolini, M.,1997. “Fusion of satellite images of different spatial resolutions: Assessing the quality of resulting images- Photogrammetric Engineering and Remote Sensing”, 63(6), pp. 691-699.

17. M. Fallah Yakhdani , A. Azizi, “Quality assessment of image fusion techniques for multisensor high resolution satellite images”, : ISPRS TC VII Symposium – 100 Years ISPRS, Vienna, Austria, July 5–7, 2010, IAPRS, Vol. XXXVIII, Part 7B